Integration of PID-MRAC and Novel GCC-C2C for Developing Adaptive Deterministic MPPT

Sidik Nurcahyo [1], Hadi Suyono [2*], Rini Nur Hasanah [3], Muhammad Aziz Muslim [4]
[1, 2, 3, 4] Department of Electrical Engineering, Faculty of Engineering, Universitas Brawijaya, Malang, Indonesia
[1] Department of Electrical Engineering, Politeknik Negeri Malang, Malang, Indonesia
Email: [1] sidiknurcahyo@student.ub.ac.id, [2] hadis@ub.ac.id, [3] rini.hasanah@ub.ac.id, [4] muh_aziz@ub.ac.id
*Corresponding Author

***Abstract*—This article proposes a new photovoltaic (PV) Maximum Power Point Tracker (MPPT) using PID-MRAC with a novel tracker of Gradual Capacitor-Charging (GCC) and Capacitor-to-Capacitor charge transfer (C2C). The research contribution is omitting the power fluctuation of optimisation-based MPPT and discontinuity or power loss of I-V sweep-based MPPT. GCC regularly and deterministically locates the maximum PV power voltage (Vmpp) by connecting a parallel capacitor to PV only when the PV is isolated from the converter. If one cycle of I-V sweeping is completed, C2C empties the capacitor by transferring its charge to a power supply capacitor to avoid the power-loss problem. A PID and non-inverting buck–boost converter was assigned to regulate the PV output voltage (Vpv) at Vmpp, thus enabling maximum energy harvesting. The Model Reference Adaptive Control (MRAC) adjusts the PID parameters to maintain the MPPT performance. Simulation results show that the MPPT worked well against load and irradiance changes, Iph=2.0A for 0.6s and Iph=3.8A for 1.4s. The GCC-C2C successfully locates Vmpp within 410ms. The PID could regulate Vpv to Vmpp with a settling time of 200ms at the initial stage or less than 10ms at the next stages. The MRAC also successfully tuned the PID parameters during operation. The superiority of this method over the P&O MPPT is its capability to deliver more power at various load power rates. Harvesting efficiency of the proposed MPPT at 5 ohm and 50 ohm loads is 96% and 82%, respectively, while P&O is only 84% and 21%.**

Keywords*—Gradual Capacitor Charging (GCC); Capacitor-to-Capacitor (C2C); Adaptive; Deterministic MPPT; PID-MRAC.

I. Introduction

The International Energy Agency (IEA) stated that more than 60% of the world's electricity was generated by power plants, which are widely known as not environmentally friendly [1]. Global warming has prompted a campaign to achieve a zero-carbon emission by 2050 [2], [3]. Various renewable energy sources (RES) have been explored to increase the capacity of green electricity, including solar power, which offers several advantages over other RES [4]–[6]. A Maximum Power Point Tracker (MPPT) is required by solar power plants or photovoltaic (PV) systems to determine the maximum power point (Pmpp), which enables the optimal harvesting of solar energy [7], [8]. MPPT can be classified into single and multiple peaks MPPT [9]–[12] . Single-peak MPPT, such as P&O [13]–[15] and INC [16], are only suitable for single-module PV systems or PV systems whose I-V curve contains only one power peak. On the other hand, the multiple-peak MPPT can be applied to multi-module PV systems as it can locate the global peak power among several local peak powers [17], [18]. This type of MPPT includes a modified P&O [19], reduced search space P&O [20], Adaptive step size P&O [21], Fuzzy [22]–[24], ANFIS [25], PPO-IC [26], MCA-FOCV [27], RP-FOSMC [28], ANN [29]–[31], PSO [32], GTO [33], GWO[34], GWO-Enhanced PSO [35], PSO, GWO-IC [36], GWO-WOA [37], Bee Colony, Heat Transfer Search [38], AFO [39], Sliding Mode Fuzzy-2 [40], Improved Sliding Mode[41], snake [42], Honey Badger [41], and many more. Most of their work relied on an optimisation algorithm. They perform well and are easy to implement [43]. However, they still result in unavoidable power losses since their Pmpp tracking is performed by testing several duty cycles (forecasted using an optimisation algorithm) directly on the converter of the PV system [44]. These losses can easily be identified by their PV voltage (Vpv) that fluctuates around the PV maximum power voltage (Vmpp) as shown in Fig. 1.

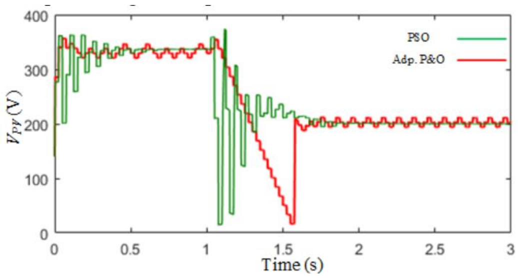

Fig. 1. PV output fluctuations caused by optimisation-based MPPT [45]

At t=0s-1s, Vmpp is 350V, and at t=1s-3s, Vmpp is 200V. Vpv of adaptive P&O (green curve) fluctuates around Vmpp both in transient and steady state. Meanwhile, the Vpv of PSO (red curve) fluctuates only in a transient state. The Vpv fluctuation contributes to the power loss of (Vmpp-Vpv) times the PV current (Ipv). This loss will be minimized if Vmpp-Vpv is reduced or Vpv does not contain fluctuation.

The I-V curve-based MPPT offers a more deterministic Pmpp tracking, without trial and error of duty cycle, thus lower losses [46]. This type of MPPT is based on photovoltaic I-V characterisation [47]–[49]. The I-V curve is obtained by measuring the PV currents and voltages while the PV system receives a varying artificial load. Several methods for generating the I-V curve have been described in [50] and [51]. These include the voltage zone (VZ), electronic load [52], series capacitors [53], parallel capacitors [54]–[56], DC-DC converters [57], and embedded parallel capacitors (EPC) [58]. VZ-based MPPT has been reported to fail to find

Pmpp if the PV system configuration is changed or if some PV modules in the PV system are damaged or short-circuited [45]. The series capacitor-based MPPT and EPC MPPT cannot be applied for large loads (draw large currents), as this causes the capacitor voltage to never reach Vmpp [58]. The DC-DC converter-based MPPT experiences high power losses because it drives the converter with a linear duty cycle ranging from 0% to 100% during its I-V sweep. Meanwhile, the parallel capacitor-based MPPT has two weaknesses: energy transfer from the PV system to the load is cut off during I–V sweeping, and power is lost when the capacitor is discharged (short-circuited to ground) [59]. Among the types of I-V tracers that can still be improved to enhance the MPPT performance is the Parallel Capacitor method. To address these two weaknesses, novel methods called Gradual Capacitor Charging (GCC) and charge transfer between capacitors (C2C) are proposed. The authors are optimistic that the successful implementation of the GCC-C2C method would become an important contribution and result in a new MPPT with a low power-loss Pmpp tracker and non-blocking energy transfer. To ensure maximum harvested energy at any time, the PV voltage should be maintained at Vmpp, i.e. the voltage determined by GCC-C2C. This requirement will be accomplished by employing a PID-MRAC controller. This controller not only regulates PV voltage output at Vmpp but also maintains its performance regardless of the plant condition, which is influenced by converter dynamics and load variation. When the plant condition is changed, these changes are detected by the MRAC, and the MRAC then re-tunes the PID parameters based on a selected reference model, thus performance will be maintained [60], [61].

The main contributions of the proposed method are reduced power losses, deterministic tracking, and converter-load adaptability, hence higher harvesting efficiency, as it can deliver more power at various loads. This principle is opposite to recent MPPT, which provides power to the load as much as required. This is possible because the proposed MPPT always tries to maintain the PV voltage (Vpv) at Vmpp. If a load suddenly changes and requires more power, as the PV system is being operated at Vmpp, then the proposed MPPT can supply the load changes faster.

II. METHODS

The MPPT development starts by constructing a block diagram, designing a circuit diagram, defining a flowchart, deriving a PID-MRAC formula, writing pseudocode, and testing the design using Proteus simulation. Its performance (transient response and harvesting efficiency) is compared to the commonly known P&O MPPT when both systems experience changes in irradiance and load.

A. MPPT Block Diagram

The MPPT block diagram is designed as shown in Fig. 2. The MPPT consists of two main parts: GCC-C2C (D4a) and PI-MRAC (D4b, D4c). The GCC-C2C traces Vmpp by sweeping the PV current and voltage. The GCC-C2C is designed to operate with negligible power losses and does not interrupt the energy transfer between the PV and load. As described by its name, GCC-C2C comprises both GCC and C2C. GCC traces Vmpp by sweeping the current and voltage of the PV system. This is achieved by connecting the PV system to the capacitor load only when the converter switch is open. C2C empties the capacitor at the end of the sweeping session by transferring the capacitor charge to the power supply capacitor. Meanwhile, the PID-MRAC is responsible for maintaining the PV voltage equal to Vmpp by adjusting the converter duty cycle. The PID parameters are tuned automatically by the MRAC; hence, the performance of maintaining Vmpp is not affected by plant parameter variations occurring in the converter or load.

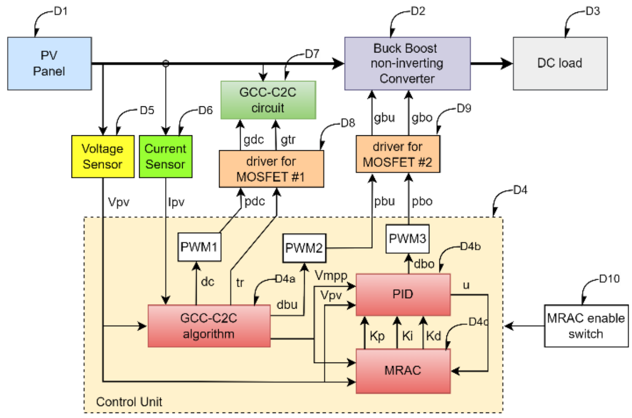

Fig. 2. Diagram for PID-MRAC MPPT using GCC-C2C tracker

Both GCC-C2C and PID-MRAC algorithms are implemented in the Control Unit (D4). This design is equipped with a voltage sensor (D5), a current sensor (D6), GCC-C2C circuit (D7), MOSFET driver for the GCC-C2C circuit (D8), and MOSFET driver (D9) for the non-inverting buck boost converter.

B. Circuit Diagram

Main MPPT circuits include the GCC-C2C and Converter as shown in Fig. 3. The GCC-C2C circuit in Fig. 3(a) comprises a capacitor C1 for I-V sweeping and C2 for charge transfer. Q1 is activated only when the converter switch Q3 is open. This forces the PV current to flow to C1, and the C1 voltage will gradually increase from zero volts to Voc (open-circuit voltage of the PV). The GCC algorithm (D4a) locates the values of Vmpp through the current and voltage measurements.

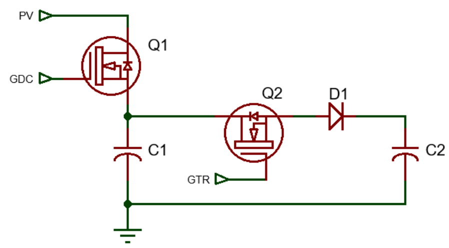

(a) Vmpp Tracker: GCC-C2C circuit

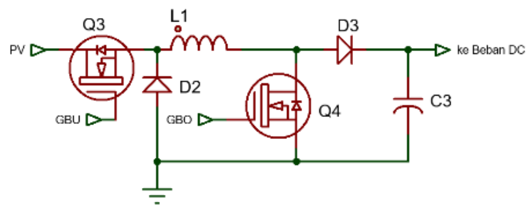

(b) Noninverting buck-boost converter

Fig. 3. MPPT circuits including Vmpp tracker and Converter

When the C1 voltage level no longer increases, the C2C algorithm empties C1 by activating Q2 shortly, hence the C1 charge is transferred to C2. If C2 is part of the power supply circuit, the transferred charge can be an additional supply for the controller circuit and is not wasted as heat, as occurred in previous studies. The circuit for D2 of Fig. 2 is shown in Fig. 3(b). Q3 is assigned to isolate PV from the remaining circuit while sweeping. Therefore, Q1 must only be activated when Q3 is open using pdc signal of Fig. 2. To prevent the C1 voltage (V_{c1}) from growing quickly, and to ensure the size of C1 is sufficiently small, C1 is designed to be charged shortly during δ as shown in Fig. 4.

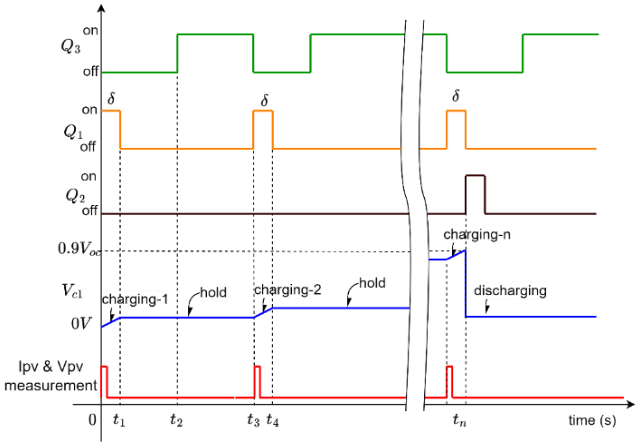

Fig. 4. Timing diagram of GCC-C2C

Each time C1 is charged, V_{c1} increases, and when Q3 is turned off, this voltage is maintained at its last level. Current and voltage were measured shortly after Q3 was turned off. When V_{c1} has reached $0.9V_{oc}$ or its level does not grow anymore, Q2 is turned on for a short duration to transfer the electrical charge from C1 to C2.

C. MPPT Flowchart

The working principle of this MPPT is fully managed by the control unit, which consists of three processes, described by the flowcharts shown in Fig. 5.

The Fig. 5(a) shows the Main process, Fig. 5(b) shows the GCC-C2C process, and Fig. 5(c) illustrates the PID-MRAC process. When starting, F1 will initialise several variables, internal modules and enable both GCC-C2C and PID-MRAC algorithms. F3 verifies the state of the MRAC enable switch (D10). If the switch is on, the MRAC variable is set as 1 using F5; otherwise, it is set as 0 using F4. Finally, F7 select one of two conditions: stop or continue running. If it is continued, to save power consumption, a 1ms delay is provided to pause execution before reevaluating the MRAC switch.

If GCC-C2C is enabled and the rising edge of the pdc signal in Fig. 2 is detected, then GCC-C2C algorithm (D4a) will be executed, or the second flowchart will be entered. This flowchart is for updating the Vmpp value. In the first step, F8 initialises several variables. F9 reads the PV voltage and current through the voltage and current sensors, respectively. It also sets the gcc variable to one to indicate that the GCC circuit is connected to the PV. This variable is used in the third flowchart of Fig. 5(c). F10 evaluates whether Vpv has reached 0.9Voc. This is done by testing the slope of Vpv or the difference between the current Vpv and the previous Vpv. If it is less than Vth, then the sweeping is completed. If so, F14 will disconnect C1 from the PV, then discharge C1 and save the last Pmpp and the last Vmpp as Pmpp and Vmpp, respectively. Otherwise, the sweeping is continued where F11 calculates the current PV power by multiplying the PV voltage and current. If the expression in F12 is true, then using F13, the flowchart assumes this power to become the last-highest power in this sweeping session.

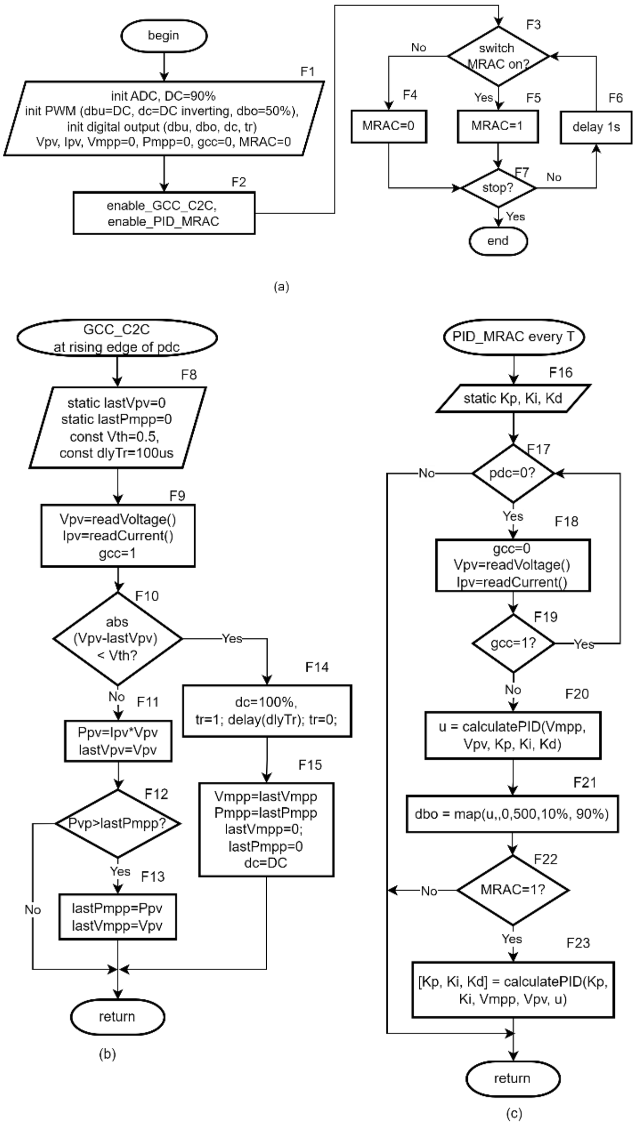

Fig. 5. Control Unit flowchart: (a) Main process, (b) GCC-C2C, and (c) PID-MRAC

If PID-MRAC is enabled, the third flowchart is entered periodically every sampling time T. Upon entering, F16 defines several static variables and then evaluates whether the pdc signal is low. If pdc is not low then it exits because the PV is connected to the GCC-C2C circuit. Otherwise, F18 will indicate that the PV is connected to a converter by clearing the gcc variable and then reading the PV current and voltage through sensors. However, if at the end of the reading of these sensors, the gcc variable changes to one, the flowchart will ignore the sensor reading because the GCC-C2C algorithm interrupts the PID-MRAC process and connects the PV to the GCC-C2C circuit. If this condition does not occur, PID-

MRAC algorithm continues to F20 that calculates PID, F21 converts the PID output into a duty cycle, and F23 runs the MRAC algorithm if F22 returns true.

D. PID-MRAC Derivation

To implement PID-MRAC in the Control Unit (D4), the PID-MRAC firstly must be derived into a mathematical formula, and then the resulting formula should be converted into a difference equation to enable the writing of code for the PID-MRAC. Assume that the plant is first order.

$$G = Y/U = b/(s+a) \tag{1}$$

Applying $df(x)/dt = pf(x)$ to (1) results in

$$py = -ay + bu \tag{2}$$

The PID controller [62], [63] is as follows:

$$U = K_pE + K_iE/s + K_dsE \tag{3}$$

Then, the plant output equation becomes

$$y = \left(pbK_p + bK_i\right)u_c/((1+bK_d)p^2 + \left(a+bK_p\right)p + bK_i) \tag{4}$$

Its gain is one and its zero is at $p = -K_i/K_p$. To match this, the reference model was chosen as follows:

$$G_m = Y_m/U_c = \alpha s + \omega_m^2/(s^2 + 2\zeta\omega_m + \omega_m^2) \tag{5}$$

Hence ouput model is as follows.

$$y_m = (ds + \omega_m^2)u_c/(p^2 + 2\zeta\omega_m p + \omega_m^2) \tag{6}$$

It has zero at $s = -\omega_m^2/d$. To guide the plant to follow the reference model, we applied the following:

$$K_i = \omega_m^2(1+bK_d)/b;\ K_p = d(a+bK_d)/b \tag{7}$$

However, this equation is not applicable, because *a* and *b* are unknown. MRAC adaptation uses the reference model output (y_m), plant output (y) and setpoint (u_c) to adjust the parameters θ (K_p, K_i, and K_d) such that the plant output is equal to the reference model output or the squared error of $\varepsilon = y - y_m$ is minimised. In this case, the cost function is

$$J = 0.5\ \varepsilon(\theta)^2 \tag{8}$$

Minimize (8) using the MIT Rule [64]:

$$d\theta/dt = -\alpha\ dJ/d\theta \tag{9}$$

and substituting ε and *J* into (9), yields:

$$\frac{d\theta}{dt} = -\frac{\alpha\varepsilon d\varepsilon}{d\theta} = -\frac{\alpha\varepsilon d(y-y_m)}{d\theta} = -\alpha\varepsilon\frac{dy}{d\theta};\quad \theta = -(\alpha\varepsilon/p)dy/d\theta \tag{10}$$

To simplify, assume $y = N/M$, $N = \left(pbK_p + bK_i\right)u_c$, and $M = (1+bK_d)p^2 + \left(a+bK_p\right)p + bK_i$. Substituting (5) into $d\theta = dK_p$, we obtain:

$$\frac{dy}{dK_p} = (pbu_cM - Npb)/M^2 = \frac{pb(u_c - y)}{M} \tag{11}$$

Derivation (5) using $d\theta = dK_i$ results in:

$$dy/dK_i = (bu_c\,M\ -\ N\,b\,)/M^2 = b(u_c - y)/M \tag{12}$$

Derivation (5) using $d\theta = dK_d$ results in:

$$\frac{dy}{dK_d} = -\frac{Nbp^2}{\mathrm{M}^2} = -\frac{bp^2y}{M} \tag{13}$$

Equation (11), (12) and (13) are unusable since M contains unknown plant parameters (a, b). Applying $\left(a+bK_p\right)/(1+bK_d)\ = 2\zeta\omega_m$ and $bK_i/(1+bK_d) = \omega_m^2$ to M yields

$$\begin{aligned} dy/dK_p &= (1+bK_d)pb(u_c - y)/(p^2 + 2\zeta\omega_m p + \omega_m^2) \\ dy/dK_i &= (1+bK_d)b(u_c - y)/(p^2 + 2\zeta\omega_m p + \omega_m^2) \\ dy/dK_d &= -(1+bK_d)bp^2y/(p^2 + 2\zeta\omega_m p + \omega_m^2) \end{aligned} \tag{14}$$

Combining (13) into (10) yields

$$\begin{aligned} K_p &= -\alpha b(1+bK_d)/p\ \cdot \varepsilon p/(p^2 + 2\zeta\omega_m p + \omega_m^2)\cdot(u_c - y) \\ K_i &= -\alpha b(1+bK_d)/p\cdot\varepsilon\cdot 1/(p^2 + 2\zeta\omega_m p + \omega_m^2)\cdot(u_c - y) \\ K_d &= \alpha b(1+bK_d)/p\cdot\varepsilon p^2/(p^2 + 2\zeta\omega_m p + \omega_m^2)y \end{aligned} \tag{15}$$

Normalizing the model gain by putting ω_m^2 in the numerator and normalizing the bandwidth by replacing p with p/ω_n produces K_p as follows:

$$K_p = \frac{-\alpha b(1+bK_d)}{p/\omega_m}\left(\frac{\varepsilon}{\omega_m}\right)\frac{p\omega_m^2(u_c - y)}{p^2 + 2\zeta\omega_m p + \omega_m^2} \tag{16}$$

and K_i was obtained as follows:

$$K_i = \frac{-\alpha b(1+bK_d)}{p/\omega_m}\varepsilon\frac{\omega_m^2(u_c - y)}{p^2 + 2\zeta\omega_m p + \omega_m^2} \tag{17}$$

and produces K_d as follows:

$$K_d = \frac{\alpha b(1+bK_d)}{p/\omega_m}\left(\frac{\varepsilon}{\omega_m^2}\right)\frac{p^2\omega_m^2 y}{p^2 + 2\zeta\omega_m p + \omega_m^2} \tag{18}$$

The K_p, K_i, and K_d formulas still contain an unknown parameter, b. This problem can be addressed by introducing $\gamma = \alpha b(1+bK_d)\omega_m$, which is a constant chosen to determine the adaptation speed of PID parameters. This results in the following adaptation formulas:

$$\begin{aligned} K_p &= -(\gamma\varepsilon/\omega_m)/p\ \cdot p\omega_m^2\cdot(u_c - y)/(p^2 + 2\zeta\omega_m p + \omega_m^2) \\ K_i &= -\gamma\varepsilon/p\cdot\omega_m^2/(p^2 + 2\zeta\omega_m p + \omega_m^2)\cdot(u_c - y) \\ K_d &= \gamma(\varepsilon/\omega_m^2)/\mathrm{p}\cdot p^2\omega_m^2/(p^2 + 2\zeta\omega_m p + \omega_m^2)\cdot y \end{aligned} \tag{19}$$

To implement these formulae in a microcontroller program, they need to be converted into discrete forms using a bilinear transform through two stages: the model reference part and the remainder part. Assume that the model reference is:

$$h = \omega_m^2 e/(p^2 + 2\zeta\omega_m p + \omega_m^2) \tag{20}$$

Using assumption $2\zeta\omega_m = a_m;\ \omega_m^2 = b_m;\ e = (u_c - y)$.

$$h/e = b_m/(p^2 + a_m p + b_m) \tag{21}$$

Substitute the following bilinear transformation [65]

$$p \leftarrow \frac{K(1-z^{-1})}{1+z^{-1}};\ K = \frac{2}{T} \tag{22}$$

into (19) to result in

$$h/e = (b_m + 2b_m z^{-1} + b_m z^{-2})/(K^2 + a_m K + b_m + (2b_m - 2K^2)z^{-1} + (K^2 - a_m K + b)z^{-2}) \quad (23)$$

The discrete form of the model reference part is as follows:

$$h(k) = \Big(-(2b_m - 2K^2)h(k-1) - (K^2 - a_m K + b_m)h_i(k-2) + b_m\big(e(k) + 2e(k-1) + e(k-2)\big)\Big)/(K^2 + a_m K + b_m) \quad (24)$$

Hence, the difference equation for K_i is

$$K_i = A_i h/p;\; K_i = A_i h(K(1-z^{-1})/(1+z^{-1}))^{-1}$$
$$K_i = (A_i/K)(1+z^{-1})h + z^{-1}K_i \quad (25)$$
$$K_i(k) = (A_i/K)(h(k) + h(k-1) + K_i(k-1)$$

where $A_i = -\gamma\,\varepsilon = -\gamma\big(y(k) - y_m(k)\big)$.

The difference equation for K_p is

$$K_p/h_i = A_p;\; K_p(k) = A_p h(k) \quad (26)$$

where $A_p = -\gamma\varepsilon/\omega_m \;= -\gamma\big(y(k) - y_m(k)\big)/\omega_m$.

The difference equation for K_d is

$$K_d/\mathrm{h} = A_d K(1-z^{-1})/(1+z^{-1})$$
$$K_d = A_d K(1-z^{-1})h - K_d z^{-1} \quad (27)$$
$$K_d(k) = A_d K\big(h(k) - h(k-1)\big) - K_d(k-1)$$

A_d dan y_m are calculated as follows.

$$A_d = -\gamma\varepsilon/\omega_m^2 = -\gamma\big(y(k) - y_m(k)\big)/\omega_m^2$$
$$y_m(k) = (2 - a_m T)y_m(k-1) + (-1 + a_m T - b_m T^2)y_m(k-2) + b_m T^2 u_c(k-2) \quad (28)$$

where $a_m = 2\zeta\omega_m$, $b_m = \omega_m^2$, and T is the sampling time. The next step was to determine the proportional-integral-derivative (PID) formula. The PID transfer function is:

$$U = K_p E + K_i E/p + K_d E\,p \quad (29)$$

Using the following backward Euler discretization [66].

$$p \leftarrow (1 - z^{-1})/T \quad (30)$$

Equation (29) can be converted to the discrete form:

$$U = K_p E + K_i ET/(1 - z^{-1}) + (K_d/T)(1 - z^{-1})E \quad (31)$$

or to the following difference equation:

$$U(k) = P(k) + I(k) + D(k)$$
$$P(k) = K_p e(k)$$
$$I(k) = I(k-1) + K_i T e(k) \quad (32)$$
$$D(k) = (K_d/T)(e(k) - e(k-1))$$

E. Pseudocode for PID-MRAC

The PID-MRAC formulas include (25), (26), (27), and (32). These equations can be implemented into pseudocode, as shown in Listing 1. Lines 2-7 define several constants. Line 8 reads the setpoint (u_c). Line 9 reads the plant output (y). Line 10 calculates the reference model output (y_m). Line 11 and line 12 calculate errors ($u_C - y$) and $\varepsilon = y - y_m$, respectively. Line 13 calculates $h(k)$. Lines 14-16 update PID parameters Kp, Ki, and Kd.

Listing 1 Pseudocode for PID-MRAC

```
1  pid_mrac:
2    const
3      T=0.01; K=2/T; gamma=0.2
4      wm=10; zeta=1.0; am=2*zeta*wm; bm= wm*wm
5      yA=(2-am*T);yB=(-1+am*T-bm*T*T); yC=bm*T*T
6      hA=-(2*bm-2*K*K);
7      hB=-(K*K-am*K+bm);hC=K*K+am*K+bm
8    uc=read_uc()
9    y=read_y()
10   ym= yA*ym1 + yB*ym2 + yC*uc2
11   e=uc-y
12   eps=y - ym
13   h=(hA*h1 + hB*he2 + bm*(e+2*e1+e2))/hC
14   Ki=-gamma*eps*he/K + Ki1
15   Kp=-gamma*(eps/wm)*K*h
16   Kd=-gamma*(eps/(wm*wm))*K*(h-h1)-Kd1
17
18   P=Kp*e
19   I=I1 + Ki*T*e
20   D=Kd*(e-e1)/T
21   u=P+I+D
22   setActuator(u)
23
24   e2=e1; e1=e
25   h1=h;
26   Ki1=Ki
27   Kd1=Kd
28   I1=I
29   uc2=uc1; uc1=uc
30   ym2=ym1; ym1=ym
```

Lines 18-21 calculate the PID formula and line 22 sends the result to the actuator. Lines 24-30 update the states of all the variables. This pid_mrac function must be executed once every fixed time interval T defined in Line 3. To make this possible, a particular timer overflow interrupt in the Control Unit should be appropriately configured to call this function.

III. Results and Discussion

This section discuss the results of GCC-C2C, PID-MRAC, the proposed MPPT and its comparison with P&O MPPT. The commonly known P&O MPPT is used as comparison. Proteus simulation was used for these purposes as it can simulate a microcontroller running an MPPT C/C++ code [67]–[71]. This will result in a more realistic response compared to other simulation programs like Matlab [72]–[75] or PSIM [76]–[78].

A. GCC-C2C Result

Complete PV system in Proteus using GCC-C2C, non-inverting buck boost converter, power supply circuit and load can be constructed as in Fig. 6. This simulation leverages the PV model developed by Mutohhir [79] and Ahmed Azi [80] that is receiving irradiance signal IR. As shown in Fig. 6(b), it is a single-diode 60WP PV model with a constant temperature of 25°C, $V_{oc} = 23.2V$ and $I_{sc} = 3.8A$. As depicted by Fig. 6(a), the PV current is measured using ACS712 where its analog output is read by AVR Atmega328 through internal ADC module. PV voltage is also measured by AVR using internal ADC module. The MPPT algorithm is implemented in C programming code and run on AVR microcontroller Atmega328 operated at highest clock of

16MHz. Pin allocation for various pheripherals is shown in Fig. 6(c). Meanwhile, C code for GCC-C2C is typed directly in the Source Code tab of Proteus, as shown in Fig. 6(d).

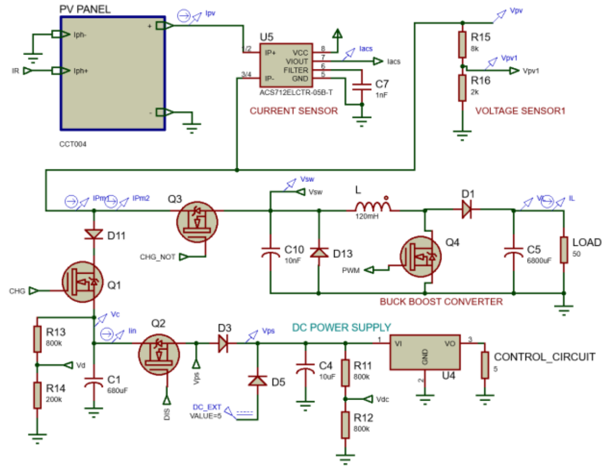

(a) Hardware circuit

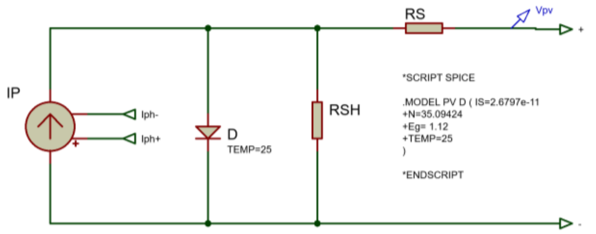

(b) Internal circuit for PV PANEL

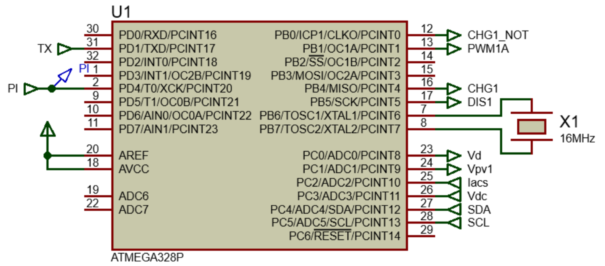

(c) Microcontroller pin allocation

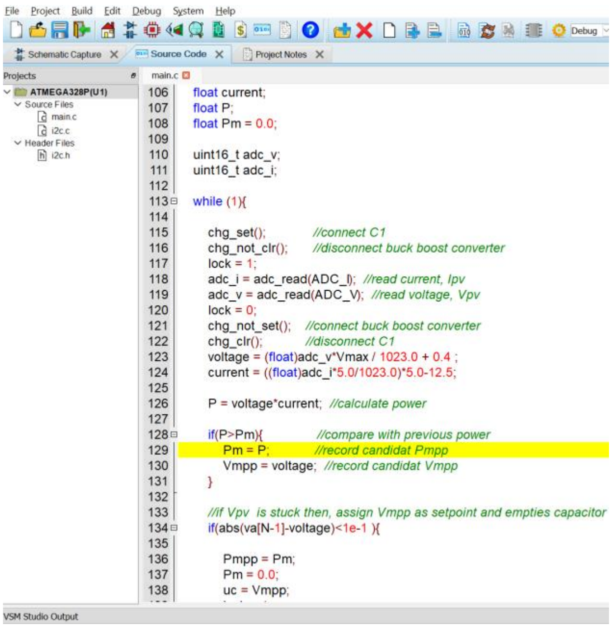

(d) Microcontroller code

Fig. 6. Complete PV system for testing

Running this simulation results in response shown in Fig. 7. This figure includes six signals describing the working principle of GCC-C2C: photon current (Iph), charge pulses (Chg), voltage stair of C_1 (Vc), current pulse flowing into C_1 (Ic), discharge pulse or transfer pulse (dis), and the GCC-C2C result (Vmpp). This figure shows 4 cycles of Vmpp tracking, indicated by stair1, stair2, stair3 and stair4.

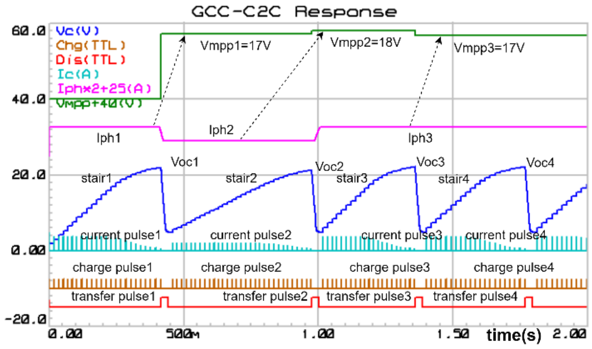

Fig. 7. GCC-C2C response

The first tracking was performed from the beginning until 410ms, which tracked Vmpp when the PV irradiance is 1000W/m^2 or Iph1=3.8A. As depicted by the Vmpp curve, the first tracking results in Vmpp1=17V at the end of the first tracking period (t=410ms). The second tracking started immediately after completing the discharging of C_1. As can be seen, the second tracking results in a higher Vmpp than the first, i.e. Vmpp=18V. At that moment, the PV irradiance produces Iph2=2A, which is lower than Iph1. The third tracking result was equal to the first tracking because the third Iph was equal to the first Iph. This result proves that GCC-C2C works as expected, where Vmpp can be obtained through the capacitor charging and discharging mechanism. Here, there is no need to test GCC-C2C against PV parameter changes, temperature variation, and partial shading phenomenon, as they will be reflected directly in the Vmpp value, and their effect is detected by GCC-C2C.

B. PID-MRAC Result

PID code implementation for (32) is shown in Fig. 8. The function pid() is attached to the ISR timer overflow 1ms to realise an accurate and constant sampling time.

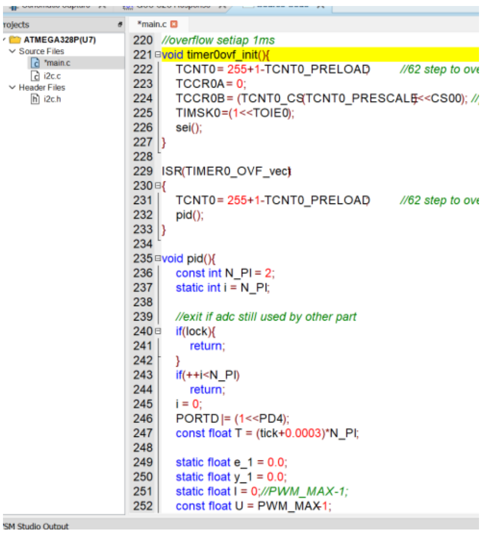

Fig. 8. Snipped code for managing PID execution via timer interrupt

If LOAD in Fig. 6(a) was set to 10 Ω and IR or Iph to 3.8A (equivalent to 1000W/m2 irradiance), resulting response shown in Fig. 9. This graph consists of six signals: PID execution indicator (PID), capacitor stair (Vc), duty cycle produced by the PID (duty), power consumed by load (PL), GCC-C2C output (Vmpp), and PV voltage (Vpv). The PID indicator appears regularly and the Vc curve that is similar to Vc in Fig. 7, indicating that the PID algorithm has been successfully worked in parallel with GCC-C2C.

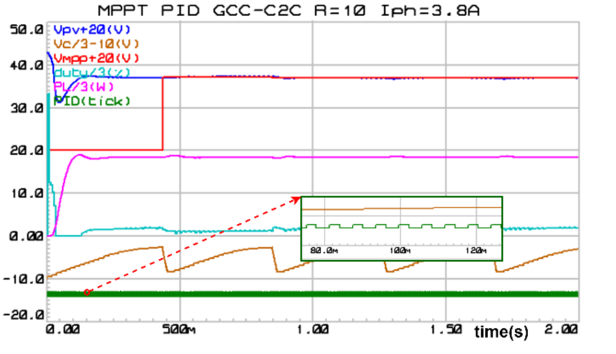

Fig. 9. The PID GCC-C2C response (R=10Ω and Iph=3.8A)

The PID can maintain Vpv equal to Vmpp with an initial settling time of 200ms by driving the boost converter with particular duty-cycles; hence, the delivered power to load is maximum, i.e. 55.8 W, whereas in this condition, the PV produces Iph=3.8A or P=60 W. The PL curve without flicker indicates that GCC-C2C can address the power supply interruption.

To evaluate the PID effectiveness, two tests have been conducted using load R=5Ω dan R=10Ω. Irradiance is dropped from Iph=3.8A to Iph=2.0A at t=400ms and recovered at t=1s, with response as shown in Fig. 10.

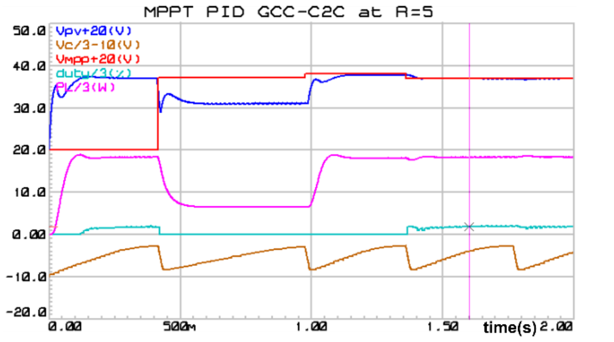

(a) PID GCC-C2C with load R=5 ohm

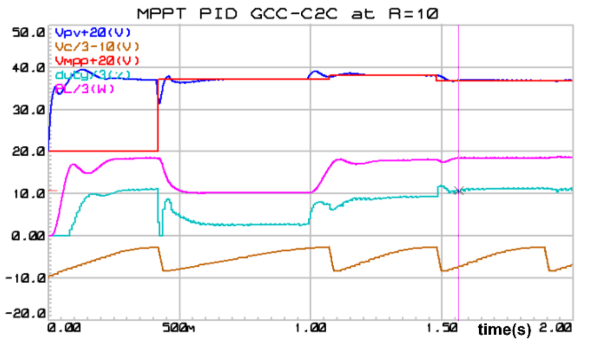

(b) PID GCC-C2C with load R=10 ohm

Fig. 10. PID GCC-C2C response (R=5Ω and R=10Ω)

When R=5Ω the Vpv deviates largely from Vmpp at t=400ms-1s because at these moments Iph drops deeply from Iph=3.8A to Iph=2.0A. The PID attempted to recover Vpv by setting the duty until it was stuck at 0%, but it still failed, as the load was too large or the resistance was too small and irradiance (Iph) was low enough. For comparison, if irradiance is increased, with Iph=3.0A, then Vpv is better in approaching Vmpp as shown in Fig. 11.

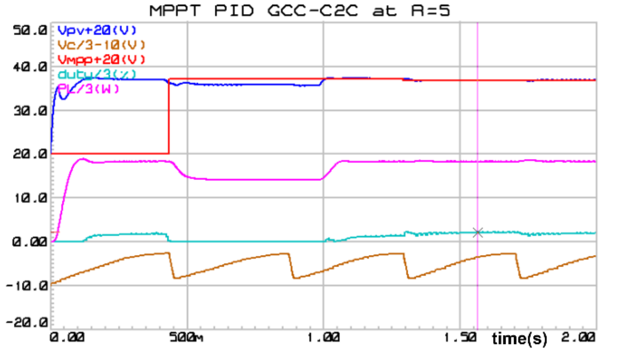

Fig. 11. PID GCC-C2C with load R=5 ohm and irradiance Iph2=3.0A

When Iph returns to the normal condition (at t=1s Iph=3.8A), Vpv can be recovered and coincides Vmpp within 10ms. This signifies that the proposed MPPT can not regulate Vpv to Vmpp if generated power is less than required power by load. However this indicates that the PID worked as expected and PID is more successful in regulating Vpv if R=10Ω, compared with R=5Ω. The power consumed by load is shown by PL curve. Fig. 10(b) shows higher level of PL (at 10), not at 6 as in Fig. 10(a). Again, this indicates that the lighter the load, the easier the Vpv stabilisation; hence, higher energy is harvested. A comparison of the Vpv curves on these graphs shows that the load resistance influences the transient response, particularly the settling time and overshoot. This occurs as the load resistance is part of the plant to be controlled by the PID, which in this case includes a converter and the load. To reduce the negative effect on MPPT performance, the PID parameters are adjusted automatically using MRAC; hence, the time-response characteristics can be maintained. Fig. 12 shows the MRAC testing results when the PID parameters were adjusted.

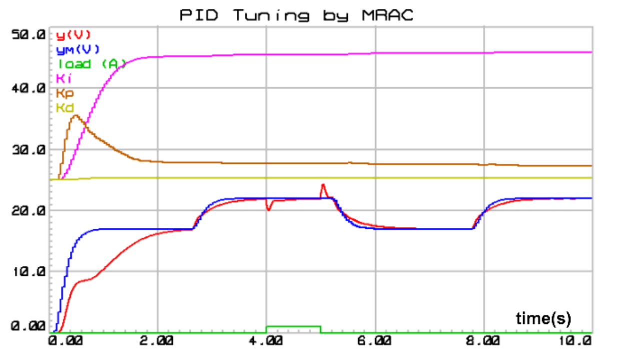

Fig. 12. MRAC response while auto-tuning PID parameters

This response shows that the PID parameters were successfully adjusted to the correct value during operation. This is proved by parameter graphs (K_p, K_i and K_d) that are settled at a particular value in 2s even though their initial values are zero. The y curve that always follows the y_m curve is also evidence that MRAC has successfully tuned the PID parameters. This mechanism will maintain the PID time response and hence the MPPT performance.

C. Comparison of the Proposed Method to the P&O MPPT

To evaluate the contribution of the proposed MPPT, response comparisons are performed with the response of the P&O MPPT. Fig. 13 shows a response comparison between P&O and the proposed MPPT using static load R=5Ω and R=10Ω. Fig. 13(a) and Fig. 13(c) is for P&O and Fig. 13(b) and Fig. 13(d) is for the proposed MPPT.

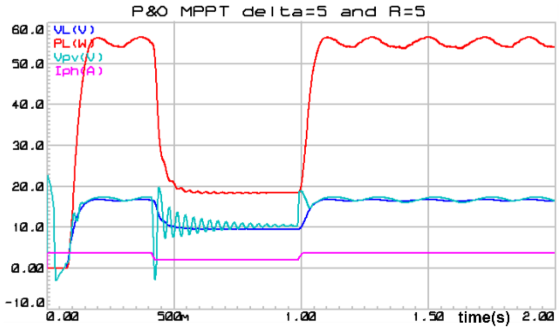

(a) P&O with load R=5 ohm

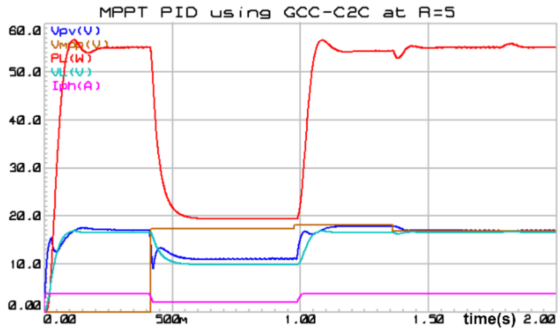

(b) GCC-C2C with load R=5 ohm

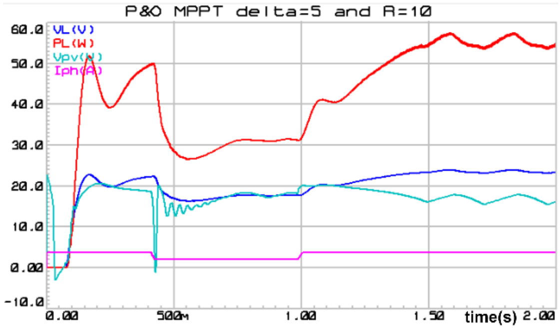

(c) P&O with load R=10 ohm

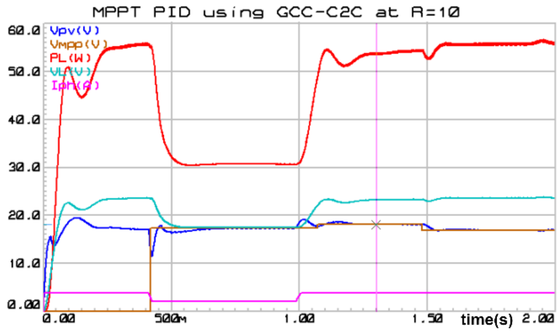

(d) GCC-C2C with load R=10 ohm

Fig. 13. Response comparison between P&O and proposed MPPT for a load R=5Ω and R=10Ω

When irradiance drops deeply from Iph=3.8A to Iph=2.0A at t=400ms, Fig. 13(a) shows that the power level PL of P&O is less than 20W, but the power level PL of the proposed method of Fig. 13(b) closer to 20W. This indicates that the proposed method can harvest more power than the P&O method. In the steady-state condition, P&O of Fig. 13(a) contains persistent fluctuation, while GCC-C2C of Fig. 13(b) does not. This is one of the superiorities of the proposed method regarding the quality of harvested energy. Tracking speed of MPPT can be evaluated through the settling time of PL against irradiance changes. When PV irradiance or Iph is changed from Iph=2.0 to 3.8A at t=1s, the P&O response in Fig. 13(c) is settled to 55 W in 0.6s, while the proposed method in Fig. 13(d) is settled in 0.2ms (3 times faster). This evidence shows that the tracking speed of the proposed method is better than P&O. A worse condition for the P&O MPPT occurred when load R=500Ω, as shown in Fig. 14.

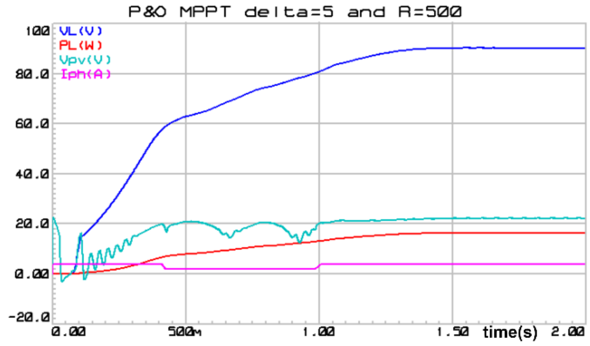

(a) P&O with load R=500 ohm

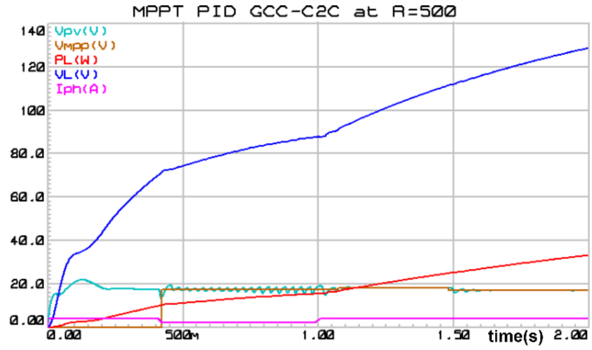

(b) GCC-C2C with load R=500 ohm

Fig. 14. Response comparison P&O vs proposed for R=500Ω

In this case, the P&O of Fig. 14(a) is failed to harvest the maximum power, as the PL curve settles only at 15 W, whereas the proposed method of Fig. 14(b) can reach 32 W at t=2s and it will grow up until the maximum power. This response indicates one of the most significant contributions of the proposed MPPT. It is more succesfully in delivering power both under low or high resistance loads. This is possible as Vpv in the proposed method is maintained to equal Vmpp.

Fig. 15 shows a response comparison between P&O and the proposed MPPT when load R changes from 50Ω to 10Ω at t=1s. Testing was done with PV irradiance 1000W/m^2 or Iph=3.8A. As depicted in Fig. 15(b), the proposed MPPT can recover power harvesting to 56.2W in 0.7s. Meanwhile, in Fig. 15(a), P&O requires a longer duration, 0.9s, and lower harvested power, 52.5 W. This confirms the superiority of the proposed MPPT against dynamic load.

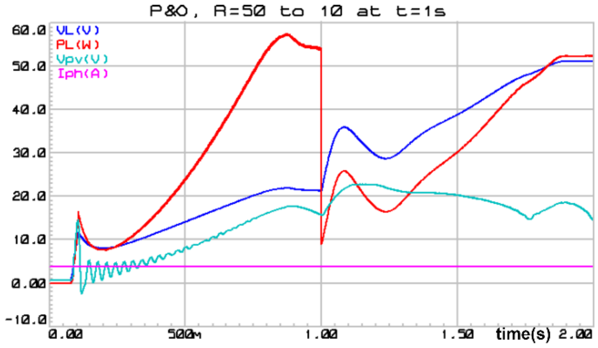

(a) P&O with load change R=50 ohm to 10 ohm at t=1s

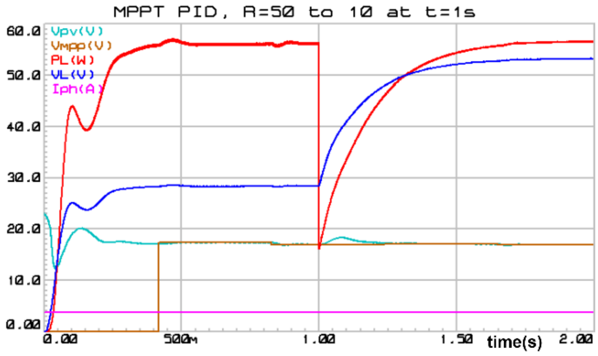

(b) GCC-C2C with load change R=50 ohm to 10 ohm at t=1s

Fig. 15. Response comparison P&O vs proposed when load changed

Regarding the power loss of capacitor discharge, in the conventional capacitor-based MPPT can be calculated using the formula $W = CV_{oc}^2/2$. Using PV PANEL in this paper ($V_{oc} = 23.2V$, $I_{sc} = 3.8A$), and the sweeping capacitor is 16000μF, which is calculated based on Fig. 6 in [54], thus W=4.31J per sweep. If this formula is applied to the proposed MPPT, but using $C = C_1$ of Fig. 6(a). i.e. $680\mu F$, then power loss W=0.183J per sweep or 4,25% of the conventional capacitor-based MPPT. This is not the actual power loss in the proposed method, as the proposed method does not discharge the capacitor to ground, but it transfers the capacitor charge to the power supply capacitor; then the actual loss will be a small portion of the power dissipated in Q2 and D3 of Fig. 6(a). If it is assumed that the dissipated power is 10% of the transferred power to C4 of Fig. 6(a), then the power loss is 0,425% of the conventional capacitor-based MPPT. So, the power loss of the proposed method is negligible.

The last but most important thing to be investigated is the amount of harvested energy and its efficiency. To do this, the harvested powers during simulation (2s) are integrated and compared to know which method will produce higher total energy, as presented in Table I. Harvesting efficiency (Eff.) is calculated by comparing W to the ideal total energy for 2s (during simulation), i.e. 103.92J (from t=0.4s to 1s is 0.6s × 33.2W = 19.92J, and for the remaining duration is 1.4s × 60W = 84J). These data show that P&O power production is worse at highly resistive loads. However, the proposed method is superior at various loads. At a 50 ohm load, P&O harvested energy is only 22.16J or 21%, while the proposed method is higher, 84.83J or 82%. At a 5 ohm load, P&O harvested energy is only 87.37J or 84%, while the proposed method is higher, 99.89J or 96%.

TABLE I. COMPARISON OF HARVESTED ENERGY BETWEEN P&O AND THE PROPOSED MPPT FOR 2S AT VARIOUS LOAD

No	Load (ohm)	P&O		Proposed		Improvement	
		W(J)	Eff.(%)	W(J)	Eff.(%)	(J)	(%)
1	5	87.37	84	99.89	96	12.52	12.5
2	10	78.70	76	92.24	89	13.54	14.6
3	20	44.13	42	90.57	87	46.44	51.2
4	50	22.16	21	84.83	82	62.67	73.8

This is possible because the proposed method repeatedly tracks Vmpp and regulates Vpv to be equal to Vmpp. Since the location of Vmpp does not depend on the load value, the harvesting performance of the proposed method depends solely on the controller performance used to regulate Vpv. The smaller the error between Vpv and Vmpp, the greater the harvested energy.

Even though the computational aspect of the proposed method is more complex (340 lines of code) than P&O (212 lines of code), the energy consumed by the microcontroller running the algorithm is almost similar, as both are operated at the same operational voltage and clock frequency. When it is applied in large-scale PV systems, sensors and power switches capacity needs to scale up as in other MPPT, including P&O. Furthermore, this method does not need to care about PV condition influenced by irradiance changes, temperature variations, or partial shading phenomenon because GCC-C2C will easily detect their effect on Vmpp value.

IV. CONCLUSION

This article proposes PID-MRAC MPPT for photovoltaic systems using a novel maximum power point tracker called GCC-C2C. GCC is assigned to locate Vmpp without interrupting the power transfer from PV to load, and C2C is for reducing the power losses that appear in the classical parallel capacitor method. The Poteus simulation was conducted to verify the effectiveness of the MPPT. The results show that GCC-C2C has been successfully implemented on an AVR microcontroller and is capable of tracing the Vmpp. A PID code integrated into the same microcontroller can work together with the GCC-C2C algorithm to maintain Vpv equals to Vmpp. The MRAC code, which was also implemented in the same microcontroller, successfully tuned the PID parameters.

The proposed MPPT offers significant contributions to the domain of renewable energy and control engineering, especially on the harvesting of photovoltaic energy. The MPPT optimizes harvesting by regulating Vpv to follow Vmpp. This method ensures that the PV system will deliver more power at various load. This method differs from optimization-based MPPT, especially P&O, where the load affects the harvested power; the lower the load (large resistance), the lower the harvested power. The main contributions of this method is capability to deterministicly find Vmpp without interrupting power delivery to load using parallel capacitor I-V sweeping and preventing power loss due to capacitor discharging. The implementation of this method is more complicated than P&O. It requires timing accuracy for both PID and MRAC. The timing needs to be managed using a timer interrupt. Meanwhile, GCC-C2C can work based on a regular process, but it is better if its execution is triggered by an external interrupt event.

Suggested further work may include replacing PID-MRAC with other adaptive control, replacing (1) with a higher-order model, and finding a more efficient method for estimating the model parameters. The practical aspects of its application are also challenging. Real hardware testing will be an interesting topic. Improvements are needed to enhance its performance, such as increasing the sampling frequency and upgrading the microcontroller from AVR (16MHz) to ESP32 (270MHz) or STM32 (250MHz) to reduce latency. Scalability, or applying the proposed MPPT to a larger PV system, is also a challenge since it is related to power switch selection, sensors, and the effort of accuracy improvement.

ACKNOWLEDGMENT

This work was supported by the Ministry of Education and Culture Research Technology and Higher Education, Republic of Indonesia funded by PPS-PDD schema with contract number 045/E5/PG/.02.00.PL/2024 and derived number 00309.87/UN10.A0501/B/PT.01.03.2/2024.

REFERENCES

[1] IEA, "World Final Energy," worldenergydata. Accessed: Oct. 29, 2023. [Online]. Available: https://www.worldenergydata.org/world-final-energy

[2] J. D. Jenkins, M. Luke, and S. Thernstrom, "Getting to zero carbon emissions in the electric power sector," *Joule*, vol. 2, no. 12, pp. 2498–2510, 2018.

[3] Y. Zhao *et al.*, "Have those countries declaring 'zero carbon' or 'carbon neutral' climate goals achieved carbon emissions-economic growth decoupling?," *J Clean Prod*, vol. 363, p. 132450, 2022.

[4] L. Wang *et al.*, "Carbon emissions and reduction performance of photovoltaic systems in China," *Renewable and Sustainable Energy Reviews*, vol. 200, p. 114603, 2024.

[5] B. Li, Y. Tian, F. Chen, and T. Jin, "Toward net-zero carbon manufacturing operations: an onsite renewables solution," *Journal of the Operational Research Society*, vol. 68, no. 3, pp. 308–321, 2017.

[6] A. Urbina, "Sustainability of photovoltaic technologies in future net-zero emissions scenarios," *Progress in Photovoltaics: Research and Applications*, vol. 31, no. 12, pp. 1255–1269, 2023.

[7] H. M. H. Farh, A. Fathy, A. A. Al-Shamma'a, S. Mekhilef, and A. M. Al-Shaalan, "Global research trends on photovoltaic maximum power extraction: Systematic and scientometric analysis," *Sustainable Energy Technologies and Assessments*, vol. 61, p. 103585, 2024, doi: 10.1016/j.seta.2023.103585.

[8] D. Mazumdar, C. Sain, P. K. Biswas, P. Sanjeevikumar, and B. Khan, "Overview of Solar Photovoltaic MPPT Methods: A State of the Art on Conventional and Artificial Intelligence Control Techniques," *International Transactions on Electrical Energy Systems*, vol. 2024, 2024, doi: 10.1155/2024/8363342.

[9] M. A. B. Siddique, D. Zhao, A. U. Rehman, K. Ouahada, and H. Hamam, "An adapted model predictive control MPPT for validation of optimum GMPP tracking under partial shading conditions," *Sci Rep*, vol. 14, no. 1, p. 9462, 2024.

[10] R. B. Bollipo, S. Mikkili, and P. K. Bonthagorla, "Hybrid, optimal, intelligent and classical PV MPPT techniques: A review," *CSEE Journal of Power and Energy Systems*, vol. 7, no. 1, pp. 9–33, 2020.

[11] L. Yi, H. Shi, J. Liu, D. Zhou, X. Liu, and J. Zhu, "Dynamic multi-peak MPPT for photovoltaic power generation under local shadows based on improved mayfly optimization," *Journal of Electrical Engineering \& Technology*, vol. 17, pp. 39–50, 2022.

[12] J. Ji, S. Yu, T. Sun, and D. Yu, "A MPPT Method for Photovoltaic System with Multi Output Power Peaks," in *2019 IEEE 10th International Symposium on Power Electronics for Distributed Generation Systems (PEDG)*, pp. 401–406, 2019.

[13] A. B. Djilali, A. Yahdou, H. Benbouhenni, A. Alhejji, D. Zellouma, and E. Bounadja, "Enhanced perturb and observe control for addressing power loss under rapid load changes using a buck–boost converter," *Energy Reports*, vol. 12, pp. 1503–1516, 2024, doi: 10.1016/j.egyr.2024.07.032.

[14] H. S. Chatterjee and S. N. Mahato, "Modified Perturb and Observe-based MPPT control of MHPCS for single-phase power distribution positioned in remote locations," *Electrical Engineering*, vol. 106, no. 6, pp. 6893–6909, 2024, doi: 10.1007/s00202-024-02390-z.

[15] X. Li, Y. He, and M. Li, "Research on Photovoltaic Maximum Power Point Tracking Control Based on Improved Tuna Swarm Algorithm and Adaptive Perturbation Observation Method," *Energies*, vol. 17, no. 12, 2024, doi: 10.3390/en17122985.

[16] A. Chellakhi, S. El Beid, Y. Abouelmahjoub, and H. Doubabi, "An Enhanced Incremental Conductance MPPT Approach for PV Power Optimization: A Simulation and Experimental Study," *Arab J Sci Eng*, vol. 49, no. 12, pp. 16045–16064, 2024, doi: 10.1007/s13369-024-08804-1.

[17] M. S. Endiz, G. Gökkuş, A. E. Coşgun, and H. Demir, "A Review of Traditional and Advanced MPPT Approaches for PV Systems Under Uniformly Insolation and Partially Shaded Conditions," *Applied Sciences (Switzerland)*, vol. 15, no. 3, 2025, doi: 10.3390/app15031031.

[18] V. L. Mishra, Y. K. Chauhan, and K. S. Verma, "A critical review on advanced reconfigured models and metaheuristics-based MPPT to address complex shadings of solar array," *Energy Convers Manag*, vol. 269, p. 116099, 2022, doi: 10.1016/j.enconman.2022.116099.

[19] R. N. Hasanah, F. Yuniar, O. Setyawati, H. Suyono, D. R. Sawitri, and T. Taufik, "A Modified Perturb-and-Observe Control for Improved Maximum Power Point Tracking Performance on Grid-Connected Photovoltaic System," *International Journal of Technology*, vol. 15, no. 1, pp. 99–109, 2024, doi: 10.14716/ijtech.v15i1.5316.

[20] A. Harrison, C. Feudjio, C. Raoul Fotso Mbobda, and N. H. Alombah, "A new framework for improving MPPT algorithms through search space reduction," *Results in Engineering*, vol. 22, p. 101998, 2024, doi: 10.1016/j.rineng.2024.101998.

[21] A. Chellakhi, S. El Beid, and Y. Abouelmahjoub, "An improved adaptable step-size P&O MPPT approach for standalone photovoltaic systems with battery station," *Simul Model Pract Theory*, vol. 121, Dec. 2022, doi: 10.1016/j.simpat.2022.102655.

[22] S. Rafi Kiran and F. Alsaif, "A novel advanced hybrid fuzzy MPPT controllers for renewable energy systems," *Sci Rep*, vol. 14, no. 1, pp. 1–17, 2024, doi: 10.1038/s41598-024-72060-4.

[23] K. Ananda-Rao *et al.*, "MPPT Charge Controller using Fuzzy Logic for Battery Integrated with Solar Photovoltaic System," *Journal of Advanced Research in Applied Sciences and Engineering Technology*, vol. 47, no. 2, pp. 171–182, 2025, doi: 10.37934/ARASET.47.2.171182.

[24] S. S. Kumar and K. Balakrishna, "A novel design and analysis of hybrid fuzzy logic MPPT controller for solar PV system under partial shading conditions," *Sci Rep*, vol. 14, no. 1, pp. 1–17, 2024, doi: 10.1038/s41598-024-60870-5.

[25] A. M. Badea, D. Manaila-Maximean, L. Fara, and D. Craciunescu, "Maximizing solar photovoltaic energy efficiency: MPPT techniques investigation based on shading effects," *Solar Energy*, vol. 285, p. 113082, 2025, doi: 10.1016/j.solener.2024.113082.

[26] S. F. Chevtchenko, E. J. Barbosa, M. C. Cavalcanti, G. M. S. Azevedo, and T. B. Ludermir, "Combining PPO and incremental conductance for MPPT under dynamic shading and temperature," *Appl Soft Comput*, vol. 131, Dec. 2022, doi: 10.1016/j.asoc.2022.109748.

[27] M. J. Alshareef, "An Enhanced Fractional Open Circuit Voltage MPPT Method for Rapid and Precise MPP Tracking in Standalone Photovoltaic Systems," *IEEE Access*, vol. 13, 2025, doi: 10.1109/ACCESS.2025.3543327.

[28] A. B. Tadesse, E. A. Ayele, and A. O. Olonje, "Design and Analysis of Rate Predictive Fractional-Order Sliding Mode Controller (RP-FOSMC) for MPPT and Power Regulation of DFIG-based Wind

Energy Conversion System (WECS)," *Energy Reports*, vol. 8, pp. 11751–11768, Nov. 2022, doi: 10.1016/j.egyr.2022.09.026.

[29] K. Krishnaram, T. S. Padmanabhan, F. Alsaif, and S. Senthilkumar, "Performance optimization of interleaved boost converter with ANN supported adaptable stepped-scaled P&O based MPPT for solar powered applications," *Sci Rep*, vol. 14, no. 1, pp. 1–17, 2024, doi: 10.1038/s41598-024-58852-8.

[30] P. R. Bana, S. D'Arco, and M. Amin, "ANN-Based Robust Current Controller for Single-Stage Grid-Connected PV With Embedded Improved MPPT Scheme," *IEEE Access*, vol. 12, pp. 100251–100262, 2024, doi: 10.1109/ACCESS.2024.3429347.

[31] M. Mishra, P. Mahajan, and R. Garg, "Implementation and comparison of metaheuristically modified ANN MPPT controllers under varying solar irradiance conditions," *Electrical Engineering*, vol. 106, no. 3, pp. 3427–3443, 2024.

[32] T. M. Shami, A. A. El-Saleh, M. Alswaitti, Q. Al-Tashi, M. A. Summakieh, and S. Mirjalili, "Particle Swarm Optimization: A Comprehensive Survey," *IEEE Access*, vol. 10, pp. 10031–10061, 2022, doi: 10.1109/ACCESS.2022.3142859.

[33] M. M. Elymany, M. A. Enany, and N. A. Elsonbaty, "Hybrid optimized-ANFIS based MPPT for hybrid microgrid using zebra optimization algorithm and artificial gorilla troops optimizer," *Energy Convers Manag*, vol. 299, p. 117809, 2024.

[34] D. Mazumdar, P. K. Biswas, C. Sain, F. Ahmad, and L. Al-Fagih, "A comprehensive analysis of the optimal GWO based FOPID MPPT controller for grid-tied photovoltaics system under atmospheric uncertainty," *Energy Reports*, vol. 12, pp. 1921–1935, 2024, doi: https://doi.org/10.1016/j.egyr.2024.08.013.

[35] J. Águila-León, C. Vargas-Salgado, D. Díaz-Bello, and C. Montagud-Montalvá, "Optimizing photovoltaic systems: A meta-optimization approach with GWO-Enhanced PSO algorithm for improving MPPT controllers," *Renew Energy*, vol. 230, 2024, doi: 10.1016/j.renene.2024.120892.

[36] J. Li, S. Lu, and J. Yang, "Multi-Stage Cooperative Optimization Control for Photovoltaic MPPT: A High-Efficiency Gray Wolf Optimizer – Incremental Conductance Hybrid Strategy," *Energies*, vol. 18, no. 8, p. 1977, 2025.

[37] A. Zemmit *et al.*, "GWO and WOA variable step MPPT algorithms-based PV system output power optimization," *Sci Rep*, vol. 15, no. 1, pp. 1–21, 2025, doi: 10.1038/s41598-025-89898-x.

[38] L. Gong, G. Hou, and C. Huang, "A two-stage MPPT controller for PV system based on the improved artificial bee colony and simultaneous heat transfer search algorithm," *ISA Trans*, Jan. 2022, doi: 10.1016/j.isatra.2022.06.005.

[39] K. Xia, Y. Li, and B. Zhu, "Improved Photovoltaic MPPT Algorithm Based on Ant Colony Optimization and Fuzzy Logic Under Conditions of Partial Shading," *IEEE Access*, vol. 12, pp. 44817–44825, 2024, doi: 10.1109/ACCESS.2024.3381345.

[40] K. Kayisli, "Super twisting sliding mode-type 2 fuzzy MPPT control of solar PV system with parameter optimization under variable irradiance conditions," *Ain Shams Engineering Journal*, vol. 14, no. 1, Feb. 2023, doi: 10.1016/j.asej.2022.101950.

[41] N. Vázquez, Y. Azaf, I. Cervantes, E. Vázquez, and C. Hernández, "Maximum Power Point Tracking Based on Sliding Mode Control," *International Journal of Photoenergy*, vol. 2015, 2015, doi: 10.1155/2015/380684.

[42] L. gang Kong, B. Wang, D. jin Fan, S. Shi, X. Ouyang, and M. Xu, "Optimize photovoltaic MPPT with improved snake algorithm," *Energy Reports*, vol. 11, pp. 5033–5045, 2024, doi: 10.1016/j.egyr.2024.04.064.

[43] R. B. Bollipo, S. Mikkili, and P. K. Bonthagorla, "Critical Review on PV MPPT Techniques: Classical, Intelligent and Optimisation," *IET Renewable Power Generation*, vol. 14, no. 9, pp. 1433–1452, Jul. 2020, doi: 10.1049/iet-rpg.2019.1163.

[44] J. Li, Y. Wu, S. Ma, M. Chen, B. Zhang, and B. Jiang, "Analysis of photovoltaic array maximum power point tracking under uniform environment and partial shading condition: A review," *Energy Reports*, vol. 8, pp. 13235–13252, 2022, doi: 10.1016/j.egyr.2022.09.192.

[45] J. Ahmed, Z. Salam, Y. L. Then, Y. L. Then, S. Kashem, and S. B. A. Kashem, "A fast MPPT technique based on I-V curve characteristics under partial shading," *IEEE Region 10 Conference*, 2017, doi: 10.1109/tencon.2017.8228132.

[46] C. Meira Amaral da Luz, Í. Ferreira Silva, P. dos Santos Vicente, E. Moreira Vicente, F. L. Tofoli, and E. R. Ribeiro, "Maximum power point tracking technique based on sweeping the characteristic curve of the photovoltaic module," *Sustainable Computing: Informatics and Systems*, vol. 33, p. 100638, Jan. 2022, doi: 10.1016/J.SUSCOM.2021.100638.

[47] F. Soltanian, "A Stable Power Reserve Control Method in Photovoltaic Systems Using I-V Curve Characteristics," in *2019 10th International Power Electronics, Drive Systems and Technologies Conference (PEDSTC)*, pp. 487–491, 2019, doi: 10.1109/PEDSTC.2019.8697261.

[48] I. F. Silva, F. Lessa Tofoli, P. dos Santos Vicente, and E. Moreira Vicente, "Maximum Power Point Tracking Based on The Curve Sweep Method," in *2021 14th IEEE International Conference on Industry Applications (INDUSCON)*, pp. 38–45, 2021, doi: 10.1109/INDUSCON51756.2021.9529667.

[49] J. Park, Y. C. Im, and Y. S. Kim, "I-V Curve Tracer Based Intermittent Maximum Power Point Tracking for Photovoltaic System," in *2022 IEEE International Symposium on Circuits and Systems (ISCAS)*, pp. 2202–2205, 2022, doi: 10.1109/ISCAS48785.2022.9937647.

[50] Y. Zhu and W. Xiao, "A comprehensive review of topologies for photovoltaic I–V curve tracer," *Solar Energy*, vol. 196, pp. 346-357, 2020, doi: 10.1016/j.solener.2019.12.020.

[51] S. Tay, L. H. I. Lim, and Z. Ye, "Modelling and Parameter Identification Using Reduced I-V Data," *University of Glasgow*, 2017.

[52] A. N. Suresh, B. Naveen, and K. Dusarlapudi, "Design and Implementation of Cost-Effective PV String IV and PV curve tracer by using IGBT as a Power Electronic Load," in *2024 6th International Conference on Energy, Power and Environment (ICEPE)*, pp. 1–7, 2024.

[53] R. Ahmad, A. F. Murtaza, U. T. Shami, Zulqarnain, and F. Spertino, "An MPPT technique for unshaded/shaded photovoltaic array based on transient evolution of series capacitor," *Solar Energy*, vol. 157, pp. 377–389, 2017, doi: 10.1016/j.solener.2017.08.025.

[54] M. M. Mahmoud, "Transient analysis of a PV power generator charging a capacitor for measurement of the I–V characteristics," *Renew Energy*, vol. 31, no. 13, pp. 2198–2206, Oct. 2006, doi: 10.1016/j.renene.2005.09.019.

[55] Y. C. Im, S. S. Kwak, J. Park, and Y. S. Kim, "Intermittent FOCV Using an I-V Curve Tracer for Minimizing Energy Loss," *Applied Sciences*, vol. 11, no. 19, p. 9006, Sep. 2021, doi: 10.3390/app11199006.

[56] F. Spertino, J. Ahmad, A. Ciocia, P. Di Leo, A. F. Murtaza, and M. Chiaberge, "Capacitor charging method for I–V curve tracer and MPPT in photovoltaic systems," *Solar Energy*, vol. 119, pp. 461–473, Sep. 2015, doi: 10.1016/j.solener.2015.06.032.

[57] A. Raj, S. R. Arya, and J. Gupta, "Solar PV array-based DC–DC converter with MPPT for low power applications," *Renewable Energy Focus*, vol. 34, pp. 109–119, 2020, doi: 10.1016/j.ref.2020.05.003.

[58] S. Selvakumar, M. Madhusmita, C. Koodalsamy, S. P. Simon, and Y. R. Sood, "High-Speed Maximum Power Point Tracking Module for PV Systems," *IEEE Transactions on Industrial Electronics*, vol. 66, no. 2, pp. 1119–1129, 2019, doi: 10.1109/TIE.2018.2833036.

[59] R. Ahmad, A. F. Murtaza, and H. A. Sher, "Power tracking techniques for efficient operation of photovoltaic array in solar applications – A review," *Renewable and Sustainable Energy Reviews*, vol. 101, pp. 82-102, 2019, doi: 10.1016/j.rser.2018.10.015.

[60] S. Manna *et al.*, "Design and implementation of a new adaptive MPPT controller for solar PV systems," *Energy Reports*, vol. 9, pp. 1818–1829, Dec. 2023, doi: 10.1016/j.egyr.2022.12.152.

[61] S. Nurcahyo, "Development of Digital PI-MRAC on Eight-Bit Microcontroller for DC-DC Boost Converter," *2024 International Conference on Electrical and Information Technology (IEIT)*, pp. 114–120, 2024, doi: 10.1109/IEIT64341.2024.10763198.

[62] I. A. Abbas and K. Mustafa, "A review of adaptive tuning of PID-controller: Optimization techniques and applications," *Int. J. Nonlinear Anal. Appl. In Press*, vol. 6822, pp. 2008–6822, 2023, doi: 10.22075/ijnaa.2023.21415.4024

[63] J. L. Guzmán and T. Hägglund, "Tuning rules for feedforward control from measurable disturbances combined with PID control: a review," *Int J Control*, vol. 97, no. 1, pp. 2–15, 2024.

[64] D. Gupta, A. Kumar, and V. K. Giri, "Effect of adaptation gain and reference model in MIT and Lyapunov rule--based model reference

adaptive control for first-and second-order systems," *Transactions of the Institute of Measurement and Control*, p. 01423312231203483, 2024.

[65] K. Talapiden, Y. Shakhin, N. G. M. Thao, and T. Duc Do, "Digital Disturbance Observer Design With Comparison of Different Discretization Methods for Permanent Magnet Motor Drives," *IEEE Access*, vol. 12, pp. 100892–100907, 2024, doi: 10.1109/ACCESS.2024.3428860.

[66] M. R. Mojallizadeh *et al.*, "Control design for thrust generators with application to wind turbine wave-tank testing: A sliding-mode control approach with Euler backward time-discretization," *Control Eng Pract*, vol. 146, p. 105894, 2024, doi: 10.1016/j.conengprac.2024.105894.

[67] T.-D. Ngo, M.-H. Nguyen, and S. Ngo, "Modeling and Simulation of Solar Energy MPPT for Arduino Using Proteus Software," in *2024 7th International Conference on Green Technology and Sustainable Development (GTSD)*, pp. 119–123, 2024.

[68] D. Bendib and M. Laour, "Modified incremental conductance MPPT using SEPIC converter for PV system, simulation and arduino implementation," *Studies in Engineering and Exact Sciences*, vol. 5, no. 2, pp. e6614--e6614, 2024.

[69] F. Moulahcene, D. Mahsoudi, A. Merazga, H. Laib, and K. Rostom, "Modeling of 100W-18V Solar Panel Using MATLAB/Simulink and Proteus Simulation," in *2024 International Conference on Electrical, Computer and Energy Technologies (ICECET)*, pp. 1–6, 2024.

[70] A. Chellakhi, S. El Beid, M. El Marghichi, E. M. Bouabdalli, A. Harrison, and H. Abouobaida, "Implementation of a low-cost current perturbation-based improved PO MPPT approach using Arduino board for photovoltaic systems," *e-Prime - Advances in Electrical Engineering, Electronics and Energy*, vol. 10, p. 100807, Dec. 2024, doi: 10.1016/J.PRIME.2024.100807.

[71] A. A. Azi, D. Saigaa, M. Drif, and A. Loukriz, "Development of generalized photovoltaic model using ISIS-PROTEUS," *Studies in Engineering and Exact Sciences*, vol. 5, no. 2, p. e5546, Jul. 2024, doi: 10.54021/seesv5n2-015.

[72] C. Restrepo, C. Gonzalez-Castano, J. Munoz, A. Chub, E. Vidal-Idiarte, and R. Giral, "An MPPT Algorithm for PV Systems Based on a Simplified Photo-Diode Model," *IEEE Access*, vol. 9, pp. 33189–33202, 2021, doi: 10.1109/ACCESS.2021.3061340.

[73] I. Saady *et al.*, "Improving photovoltaic water pumping system performance with PSO-based MPPT and PSO-based direct torque control using real-time simulation," *Scientific Reports,* vol. 15, no. 1, pp. 1–24, May 2025, doi: 10.1038/s41598-025-00297-8.

[74] H. Ahessab, A. Gaga, and B. EL Hadadi, "Revolutionizing photovoltaic power: An enhanced Grey Wolf Optimizer for ultra-efficient MPPT under partial shading conditions," *Sci Afr*, vol. 27, p. e02586, Mar. 2025, doi: 10.1016/J.SCIAF.2025.E02586.

[75] S. M. Belhadj *et al.*, "Control of three-level quadratic DC-DC boost converters for energy systems using various technique-based MPPT methods," *Scientific Reports*, vol. 15, no. 1, pp. 1–25, Apr. 2025, doi: 10.1038/s41598-025-99551-2.

[76] A. El Aroudi, G. Zhang, and M. Al-Numay, "Performance evaluation for an hourglass-shaped impedance-network-based high step-up converter in a photovoltaic system using PSIM© simulation," *International Journal of Circuit Theory and Applications*, vol. 49, no. 9, pp. 2670–2685, Sep. 2021.

[77] L. Alkhawaldeh, M. A. Bhuiya, M. Eid, and M. Z. Youssef, "An Enhanced EPP-MPPT Algorithm with Modified Control Technique in Solar-Based Inverter Applications: Analysis and Experimentation," *IEEE Access*, vol. 9, pp. 8158–8166, 2021, doi: 10.1109/ACCESS.2021.3049517.

[78] S. Manna *et al.*, "Design and implementation of a new adaptive MPPT controller for solar PV systems," *Energy Reports*, vol. 9, pp. 1818–1829, Dec. 2023, doi: 10.1016/J.EGYR.2022.12.152.

[79] S. Motahhir, A. Chalh, A. El Ghzizal, and A. Derouich, "Development of a low-cost PV system using an improved INC algorithm and a PV panel Proteus model," *J Clean Prod*, vol. 204, pp. 355–365, 2018.

[80] A. Ahmed Azi, D. Saigaa, M. Drif, A. Loukriz, A. Bendib, and M. Kichene, "Improved PV module model for dynamic and nonuniform climatic conditions in ISIS-proteus," *Electrical Engineering*, vol. 107, no. 2, pp. 2369–2389, 2024, doi: 10.1007/s00202-024-02639-7.